

# Molecular dynamics investigation of soliton propagation in a two-dimensional Yukawa liquid

Zoltán Donkó<sup>1</sup> | Peter Hartmann<sup>1</sup> | Ranna U. Masheyeva<sup>2</sup> |  
Karlygash N. Dzhumagulova<sup>2</sup>

<sup>1</sup>Institute for Solid State Physics and Optics, Wigner Research Centre for Physics, Department of Complex Fluids, Budapest, Hungary

<sup>2</sup>IETP, Department of Plasma Physics Al-Farabi Kazakh National University, Almaty, Kazakhstan

## Correspondence

Zoltán Donkó, Institute for Solid State Physics and Optics, Wigner Research Centre for Physics, Budapest, Hungary.  
Email: donko.zoltan@wigner.hu

## Funding information

Nemzeti Kutatási Fejlesztési és Innovációs Hivatal, Grant/Award Numbers: 115805, 119357; Ministry of Education and Science of the Republic of Kazakhstan, Grant/Award Number: AP05132665

## Abstract

We investigate via molecular dynamics simulations the propagation of solitons in a two-dimensional many-body system characterized by Yukawa interaction potential. The solitons are created in an equilibrated system by the application of electric field pulses. Such pulses generate pairs of solitons, which are characterized by a positive and negative density peak, respectively, and which propagate into opposite directions. At small perturbation, the features propagate with the longitudinal sound speed, from which an increasing deviation is found at higher density perturbations. An external magnetic field is found to block the propagation of the solitons, which can, however, be released upon the termination of the magnetic field and can propagate further into directions that depend on the time of trapping and the magnetic field strength.

## KEYWORDS

dusty plasma, molecular dynamics simulation, soliton propagation

## 1 | INTRODUCTION

With the pioneering observation of “wave of translation” made by John S. Russell in 1834 on the Union Canal in Scotland, the field of nonlinear wave phenomena was born. Russell continued his investigations in water channel experiments by triggering waves with translating vertical plates placed in the water.<sup>[1,2]</sup> With his experiments, he was able to determine some properties of the single (“solo” or as later called “solitary”) waves, like that those are stable features, which can travel a long distance, and that the speed of the wave depends on its amplitude and on the water depth. He also found that two waves do not disturb each other so that, for example, they can overtake each other.

Due to the lack of proper theoretical description of nonlinear wave phenomena, the field did not experience much progress for several decades. This changed with the derivation of the Korteweg–de Vries (KdV) equation in 1896,<sup>[3]</sup> which is the simplest equation embodying nonlinearity and dispersion. Despite its apparent simplicity, it is very rich and has a large variety of solutions, including spatially localized solitary waves and periodic cnoidal waves. In the meantime, solitons have been identified in many different fields beyond hydrodynamics, including optics (optical fibres and nonlinear media),<sup>[4]</sup> magnetism,<sup>[5]</sup> nuclear physics,<sup>[6]</sup> and Bose-Einstein condensates.<sup>[7]</sup>

Solitons are salient nonlinear features in plasmas too. A review of the early experimental findings of ion-acoustic solitons was published.<sup>[8]</sup> The combination of large family of systems we call plasmas and the richness of the KdV equation and its variants provides seemingly unlimited possibilities for theoretical investigations. Just to mention some of the

most recent ones, the collision properties of overtaking small-amplitude super-solitons, as well as solitons with opposite polarities in a plasma consisting of cold ions and electrons with two-temperature Boltzmann energy distributions were investigated.<sup>[9,10]</sup> The effect of relativistic corrections to the electron kinetics on wave propagation was discussed.<sup>[11]</sup> Ion acoustic solitons in multi-ion plasmas have been analysed.<sup>[12,13]</sup> Multiple soliton solutions have been presented in (3 + 1) dimensions.<sup>[14]</sup> The effect of magnetic field acting on the dust particle motion was taken into account<sup>[15–17]</sup> while solitary waves and rogue waves in a plasma with nonthermal electrons featuring Tsallis distribution have been derived.<sup>[18]</sup> Bending of solitons in weak and slowly varying inhomogeneous plasmas is shown<sup>[19]</sup> and the application of solitary waves for particle acceleration has been discussed.<sup>[20]</sup>

More closely related to the topic of this paper, in the field of strongly coupled dusty plasma research solitons became of high interest in the last decade after the pioneering experiments of Samsonov et al.<sup>[21]</sup> Numerous single-layer dusty plasma experiments have followed providing more data and insight.<sup>[22–24]</sup> The connection between wave amplitude, width, and propagation velocity has been explored,<sup>[25]</sup> the existence of dissipative dark (rarefactive) solitons has been reported.<sup>[26,27]</sup> Experiments on the collision of solitons were presented.<sup>[28]</sup> Experimental observations on the modifications in the propagation characteristics of precursor solitons due to the different shapes and sizes of obstacles over which the dust fluid had to flow is presented.<sup>[29]</sup> In three-dimensional dusty plasmas, under micro-gravity conditions solitons could be launched as well, as reported.<sup>[30]</sup> Solitary waves in one-dimensional dust particle chains were studied.<sup>[31]</sup>

Supporting and extending experimental possibilities concerning solitons in dusty plasma, theoretical studies focused on the effects of charge-varying dusty plasma with nonthermal electrons,<sup>[32]</sup> of an external magnetic field,<sup>[33]</sup> of the external periodic perturbations, and damping,<sup>[34]</sup> as well as of the presence of dust particles with opposite polarities.<sup>[35]</sup> The effects of dust–ion collision,<sup>[36]</sup> and the possibility of cylindrical solitary waves<sup>[37]</sup> were also addressed.

Numerical simulations became as well very useful for exploring the physics of strongly coupled dusty plasmas. The most widely used approach has been the molecular dynamics (MD) method, which solves the equations of motion of the particles with forces originating from the specified pairwise interparticle potential and from any external fields, if present. In many settings, the validity of the Newtonian equations of motion can be assumed. In the case of an appreciable interaction between the particles and the embedding gaseous system, the Langevin simulation approach<sup>[38]</sup> can be adopted. Recent MD simulations have shown the presence of solitary waves and their compatibility with the predictions of the KdV equation,<sup>[39,40]</sup> the possibility of excitation of solitons with moving charged objects,<sup>[41]</sup> and the presence of rarefactive solitons.<sup>[42]</sup>

Since the first laboratory plasma crystal experiments in 1994,<sup>[43–45]</sup> strongly coupled two-dimensional dusty plasmas and the corresponding single layer Yukawa one-component plasma model became popular model systems for the investigation of various structural, transport, and dynamical properties of many-body systems. These systems provide the unique possibility to observe collective and many-body phenomena on the microscopic level of individual particles. Most recent works on transport processes include studies of the effect of external magnetic fields on the different transport parameters<sup>[46–48]</sup> and testing different thermal conductivity models with equilibrium MD simulation.<sup>[49]</sup> Related to waves and instabilities, the coupling of non-crossing wave modes has been addressed,<sup>[50]</sup> spiral waves in driven strongly coupled Yukawa systems were analysed,<sup>[51]</sup> the effect of periodic substrates were studied,<sup>[52,53]</sup> thermoacoustic instabilities in the liquid phase were shown,<sup>[54]</sup> and microscopic acoustic wave turbulence was analysed.<sup>[55]</sup> Studies on structural phase transitions included freezing<sup>[56,57]</sup> and melting.<sup>[58,59]</sup>

Dusty plasmas also provide an easily accessible playground for testing new theoretical approaches and concepts. For example, the shear modulus for the solid phase was obtained from the viscoelasticity in the liquid phase,<sup>[60]</sup> a survival-function analysis was performed to identify multiple timescales in strongly coupled dusty plasma,<sup>[53]</sup> the applicability of the configurational temperature in dusty plasmas was investigated.<sup>[61]</sup> High-precision MD results were used for testing of theoretical models of ion-acoustic wave-dispersion relations and related quantities.<sup>[62]</sup> Studies at the mesoscopic scale of finite dust particle clusters are probably at the most fundamental level, as the contribution of every individual particle is significant. Most recently, amplitude instability, phase transitions, and dynamic properties were studied.<sup>[63]</sup> In addition to fundamental many-body physics, dusty plasmas provide a very sensitive tool for the detailed investigation of mutual plasma–surface interactions. Recent studies include the investigations of the effect of external fields on the local plasma properties around a dust particle,<sup>[64]</sup> and the sputtering rate of the solid dust surface with nanometre resolution.<sup>[65]</sup>

In this work, we present MD investigations of the propagation of solitons in a two-dimensional strongly coupled many body system, characterized by Yukawa pair potential. The solitons are created by electric field pulses. Their propagation and their collisions are traced at various system parameters. The effect of an external magnetic field is also addressed. In Section 2, we describe our simulation techniques, the generation and the characterization of the solitons. In Section 3, we report the results of our studies, while in Section 4 a brief summary of our findings is given.

## 2 | SIMULATION TECHNIQUE

The system that we investigate consists of  $N$  particles that have the same charge,  $Q$ , and mass,  $m$ , and reside within a square computational box, to which we apply periodic boundary conditions. The edge length of the box is  $L$  that results a surface density of the particles  $n = N/L^2$  and a Wigner-Seitz radius of  $a = (\pi n)^{1/2}$ . The particles interact via the screened Coulomb (Debye-Hückel, or Yukawa) potential

$$\phi(r) = \frac{Q}{4\pi\epsilon_0} \frac{\exp(-r/\lambda_D)}{r}, \quad (1)$$

where  $\lambda_D$  is the screening (Debye) length, which depends on the characteristics of the plasma environment (densities and temperatures of the electrons and ions) that embeds the dust system. We account for the presence of the plasma environment solely by taking into account its screening effect, that is, we assume that the friction force that originates from this plasma environment is negligible. Correspondingly, we use the Newtonian equation of motion to follow the trajectories of the particles ( $i = 1, 2, \dots, N$ ),

$$m\ddot{\mathbf{r}}_i = \mathbf{F}_i = Q\mathbf{v}_i \times \mathbf{B} + \sum_{i \neq j} \mathbf{F}_{ij}(r_{ij}) + Q\mathbf{E}^*, \quad (2)$$

where  $\mathbf{B}$  is an external magnetic field that is perpendicular to the simulation plane,  $\mathbf{F}_{ij}(r_{ij})$  is the force that acts on particle  $i$  due to its interaction with particle  $j$  situated at a distance  $r_{ij}$ , while the last term represents the force originating from the electric field  $\mathbf{E}^*$  that is used to create the density perturbations. Our studies cover both  $\mathbf{B} = 0$  and  $\mathbf{B} \neq 0$  cases. The electric field induced by switching  $\mathbf{B}$  on and off is neglected, which corresponds to modelling the centre region of a large system extending well beyond the simulation box. The characteristics of  $\mathbf{E}^*$  will be defined below. Note, that our simulations assume a frictionless system, in accordance with this no damping term appears in the equation of motion.

The summation for the interparticle forces is carried out within a domain limited by a cutoff distance,  $r_{ij} \leq r_c$ . The exponential decay of the pair potential allows us to assume that force contributions from particles at  $r_{ij} > r_c$  are negligible.  $r_c$  is set in a way to ensure that  $F(r_c)/F(2a) \sim 10^{-5}$  (recall that the nearest neighbour distance is  $\approx 2a$ ). Finding the particles that give a contribution to the force acting on a given particle is aided by the chaining mesh technique. The resolution of the chaining mesh is set to be equal to  $r_c$ .

In the cases when no magnetic field is applied, the equations of motion are integrated using the Velocity-Verlet scheme with a time step  $\Delta t$  that provides a good resolution and accuracy over the time scale of the inverse plasma frequency  $\omega_p^{-1} = (nQ^2/2\epsilon_0 ma)^{-1/2}$  (by setting  $\omega_p \Delta t = 1/30$ ). In the presence of magnetic field, the integration of the equations of motion is based on the method described in.<sup>[66]</sup>

The system is characterized by three dimensionless parameters: the coupling parameter

$$\Gamma = \frac{Q^2}{4\pi\epsilon_0} \frac{1}{ak_B T}, \quad (3)$$

where  $T$  is the temperature, the screening parameter

$$\kappa = a/\lambda_D, \quad (4)$$

and the normalized magnetic field strength

$$\beta = \Omega_c/\omega_p, \quad (5)$$

where  $\Omega_c = QB/m$  is the cyclotron frequency.

Upon the initialization of the simulations, the particles are placed at random positions within the simulation box and their velocities are sampled from a Maxwell-Boltzmann distribution that corresponds to the temperature defined by  $\Gamma$ . During the first 20,000 time steps, the system is equilibrated by rescaling in each time step the velocities of the particles to match the desired system temperature. As this type of “thermalization” produces a non-Maxwellian velocity distribution, no measurements on the system are taken during this initial phase of the simulation. This phase is followed by a “free run”

period (consisting of 10,000 time steps), during which the system is no longer thermostated and is allowed to equilibrate due to the interaction between the particles.

Following this phase, solitons in the system are created by applying an electric field pulse with a duration of  $\omega_p \Delta t = 1/6$  and having a spatial form

$$E^*(x) = \tilde{E}_0 \frac{Q}{4\pi\epsilon_0 a^2} \exp\left[-\frac{(x-x_0)^2}{2w^2}\right], \quad (6)$$

where  $x_0$  is the position where the soliton is to be generated, and  $w$  the width of the perturbation region. We set this value to  $w = 0.01L$ . The pulse is spatially homogeneous in the  $y$  direction, that is, particles with a given  $x$  coordinate experience the same force regardless of their  $y$  coordinates.  $\tilde{E}_0$  in Equation (6) is a dimensionless scaling factor that controls the strength of the perturbation: the factor  $Q/(4\pi\epsilon_0 a^2)$  ensures that at  $\tilde{E}_0 = 1$  the peak value of the perturbing force acting on a particle at  $x_0$ ,  $E^*Q$ , equals the Coulomb force between two particles separated by a distance  $r = a$ .

The application of a pulse given by Equation (6) causes a compression of the particles on the right side and a rarefaction of the particles on the left side of the interaction region of width  $w$ . The positive density perturbation propagates in the  $+x$  direction, while the negative density perturbation propagates in the  $-x$  direction, as it will be shown later.

The propagation of these structures is traced by recording the time evolution of the spatial density distribution of the particles. To facilitate this, the simulation box is split into  $M = 200$  ‘stripes’ along the  $x$  axis and the density of the particles is measured within these stripes in each time step. Density data are saved in every 20th time step for further analysis.

The operation of the simulation method is illustrated on a small system consisting of 40,000 particles. (The results in Section 3 will be given for systems consisting of 4,000,000 particles.) For this case we set  $\Gamma = 100$  and  $\kappa = 1$ , and a very high value for the perturbation field,  $\tilde{E}_0 = 8.3$  that generates density perturbations, which can easily be observed by eye on the particle snapshots. The perturbation is applied at time  $t = 0$  and at the position  $x_0 = L/2$ .

Figure 1a shows snapshots of the particle positions at a time (at  $\omega_p t = -66.7$ ) that belongs to the equilibrium phase, before the application of the electric field pulse at  $t = 0$ . Here, we find a homogeneous density distribution of the particles. Panel b shows a snapshot right after the perturbing pulse, at  $\omega_p t = 2.67$ . A strong negative/positive density perturbation ( $\delta n/n \approx 20\%$ ) is created left/right from the middle of the simulation box,  $x/L = 0.5$ , as it can also be seen in panel d of Figure 1. These perturbations propagate into opposite directions and acquire specific shapes, see for example panel c that shows a snapshot of the particle configuration at  $\omega_p t = 66.7$ . At this time, the positive density peak has a sharp leading edge, which is followed by a slow decay of the density. For the negative density peak, on the other hand, we find a slow change of the density at the leading edge and a very sharp trailing edge (also well seen in panel d). There is an obvious difference between the propagation velocities of the two structures; the velocity of the positive peak is about three times higher as compared to that of the negative peak. We note that these properties are consequences of the very high degree of perturbation, for most of our studies, we use significantly lower amplitude of the perturbing field, resulting in density perturbations in the order of  $\delta n/n \approx 1\%$ .

### 3 | RESULTS

The results presented below are derived from simulations that use  $N = 4,000,000$  particles with a chaining mesh of  $N_c = 400$ . The cutoff distance is chosen as  $r_c = L/N_c \cong 9a$ . The width of the electric field pulse used for the generation of the solitons is set to  $w \approx 35a$ . The perturbation is applied at  $x_0 = L/2$  unless specified otherwise.

In Section 3.1, simulation results are reported for nonmagnetized systems, for different  $\Gamma$  and  $\kappa$  values, as well as various perturbing electric field strength,  $\tilde{E}_0$ . ‘Collisions’ of two solitons are also investigated. In Section 3.2, the effect of an external magnetic field on the propagation of the solitons is studied.

#### 3.1 | Nonmagnetized systems

Figure 2 shows the density of the particles as a function of normalized space ( $x/L$ ) and time ( $\omega_p t$ ) coordinates, for different degrees of perturbation applied at  $t = 0$  and  $x/L = 0.5$ . At the smallest perturbation amplitude,  $\tilde{E}_0 = 0.277$ , we observe that the density changes on the scale of  $\sim 1\%$ . The propagating positive and negative perturbations of the density show up as red and blue lines on this plot. The slopes of these lines are the same, that is, both features exhibit the same velocity of propagation. At such low perturbation, low-amplitude spontaneous propagating density fluctuations are also visible

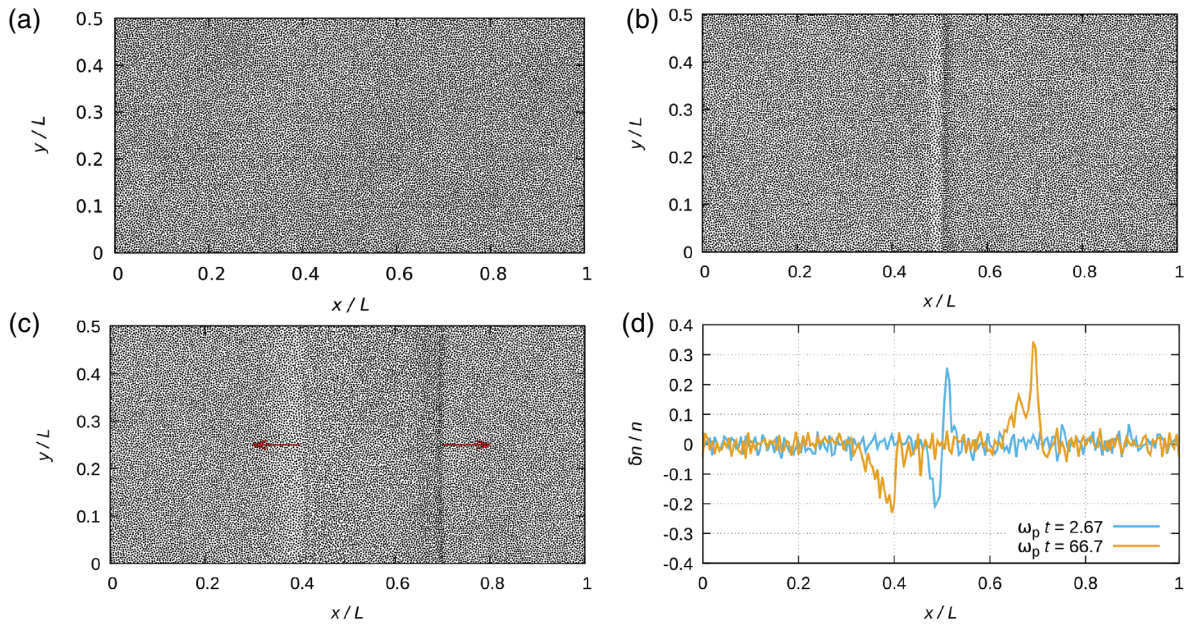


**FIGURE 1** Snapshots of the system at (a)  $\omega_p t = -66.7$  (equilibrium phase, before perturbation), (b)  $\omega_p t = 2.67$  (right after perturbation), and (c)  $\omega_p t = 66.7$  (well after perturbation). The perturbation electric field is applied at the time  $t = 0$  and at the position  $x_0 = L/2$  with an amplitude  $\tilde{E}_0 = 8.3$ . The red arrows in (c) indicate the direction of propagation of the density fronts. A positive density perturbation propagates in the  $+x$  direction, while a negative density perturbation propagates in the  $-x$  direction. (d) The density of the particles (averaged over the  $y$  direction) at  $\omega_p t = 2.67$  and  $66.7$ . The plots in (a–c) show only half of the system in the  $y$  direction.  $\Gamma = 100$  and  $\kappa = 1$ . To visualize the phenomenon studied the system is perturbed here very strongly. Note the significantly higher propagation velocity of the positive density perturbation

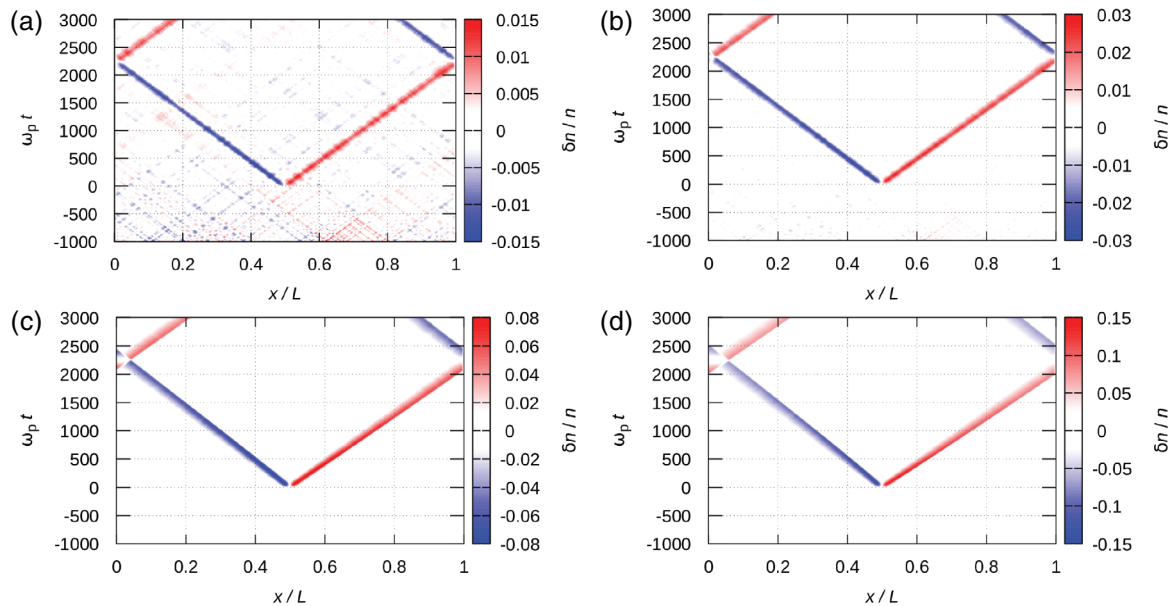


**FIGURE 2** Density of the system as a function of space and time. The perturbation electric field is applied at  $t = 0$ , at the position  $x/L = 0.5$ , with amplitudes  $\tilde{E}_0 = 0.277$ , (a),  $0.554$  (b),  $1.662$  (c), and  $2.77$  (d).  $\Gamma = 100$  and  $\kappa = 1$ . As an effect of the periodic boundary conditions the solitons that leave the simulation box at either side, re-enter the box at the opposite side. Note, that while at low  $\tilde{E}_0$  the positive and negative density peaks propagate with the same velocity, with increasing  $\tilde{E}_0$  the velocity of the positive density peak becomes higher, and the velocity of the negative peak becomes lower. The additional features seen in (a) correspond to low-amplitude, spontaneous, propagating density fluctuations in the system

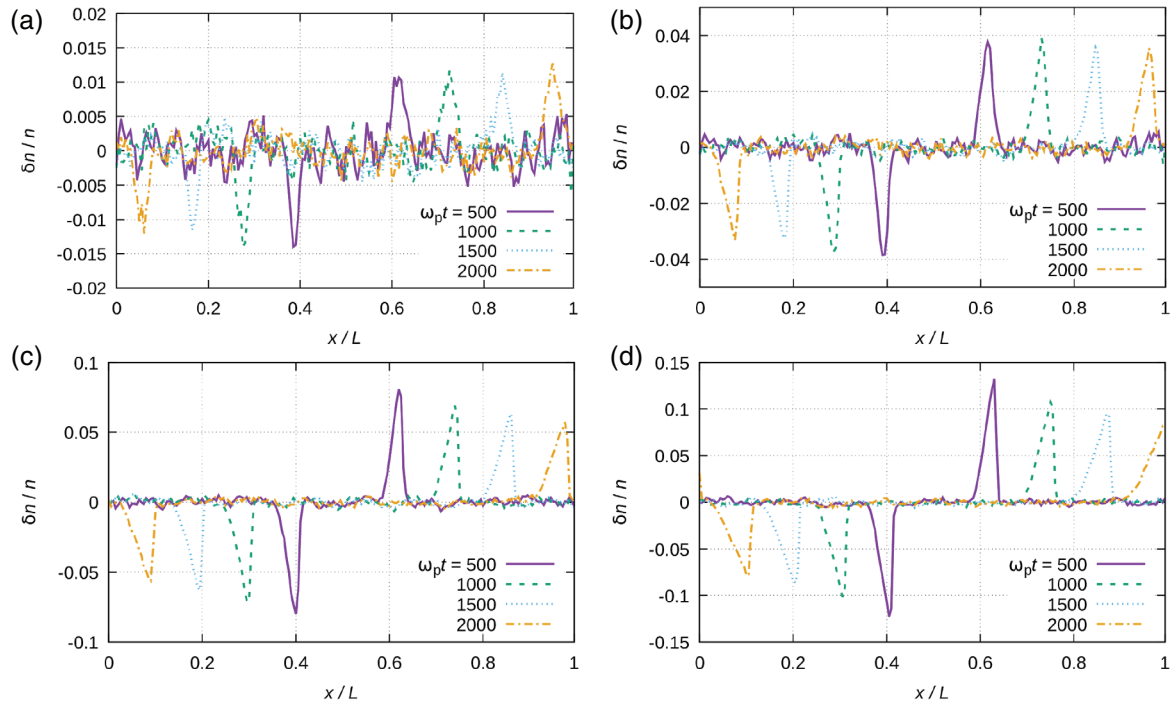


**FIGURE 3** Density of the system as a function of space at different times following the application of the perturbation electric field,  $\tilde{E}_0 = 0.277$  (a), 0.554 (b), 1.662 (c), and 2.77 (d). The perturbation electric field pulse is applied at  $t = 0$ , at the position  $x/L = 0.5$ .  $\Gamma = 100$  and  $\kappa = 1$

to some extent. These features have the same propagation speed as the generated solitons. Similarly, to the solitons, the spontaneous features have as well two branches that are created upon the initialization of the simulations.  $\delta n/n$  in these two branches is, however, the same, unlike in the pairs of solitons that are created by the electric field pulse defined by Equation (6). At higher degrees of perturbation (Figure 2b–d) these features are no longer observed due to the broader range of  $\delta n/n$  of interest. At these conditions, the propagation velocities of the “+” and “−” solitons becomes unequal: while at low  $\tilde{E}_0$  (see Figure 2a), the features “meet” at the sides of the simulation box, at higher  $\tilde{E}_0$  the positive peak propagates with a higher velocity compared to the negative peak.

The strength of the perturbation,  $\tilde{E}_0$ , also influences the shapes of the propagating density perturbations. This is shown in Figure 3, which displays cuts of the density profiles at given times. For the case of  $\tilde{E}_0 = 0.277$  the two peaks propagate symmetrically in both directions and have similar shapes. The different propagation velocities are confirmed here, too, for the amplitudes  $\tilde{E}_0 = 0.554$ , 1.662, and 2.77 (panels b–d, respectively). At high perturbations, the shapes of both density peaks become significantly different. The positive density peak acquires a sharp leading edge and an extended trailing edge, while the opposite happens for the negative density peaks. At  $\tilde{E}_0 = 0.277$  and 0.554 (Figure 3a,b) the amplitude of the propagating peaks decreases only slightly with time, which is due to the broadening of the density “pulses”. At higher perturbations, a significant broadening as well as a remarkable change of the pulse shapes is seen in panels c and d of Figure 3. These effects, actually, can also be revealed from the spatio-temporal distributions shown previously in Figure 2.

Our further studies are conducted with an electric field amplitude of  $\tilde{E}_0 = 0.554$ , which represents a compromise between the signal to noise ratio and small change of the density peak shapes with time. At lower  $\tilde{E}_0$  we have observed density peaks in the order of 1% which is not much higher than the “natural” fluctuations of the density in the slabs where the density is measured. (As we use 200 slabs, the average number of particles in these is 20,000, resulting in a fluctuation level of  $\sim 1/\sqrt{20,000} \approx 0.7\%$ .) At high  $\tilde{E}_0$  values, we have observed a significant change of the shapes of the density peaks over an extended domain of time.

Figure 4, together with Figure 2b illustrates the effect of the screening parameter  $\kappa$ , on the propagation of the solitons. The softening of the potential (i.e., an increasing  $\kappa$ ) clearly results in a decrease of the propagation velocity. In the limit of small amplitude, solitons are found to propagate with the longitudinal sound speed. This is confirmed in Figure 5a that shows the measured propagation velocities as a function of  $\kappa$ , in comparison of the theoretical curve derived from lattice summation calculations. The measured data are shown for both the positive and the negative density peaks, the first of these always indicates a slightly higher velocity. Figure 5b shows the propagation velocity of the solitons as a function

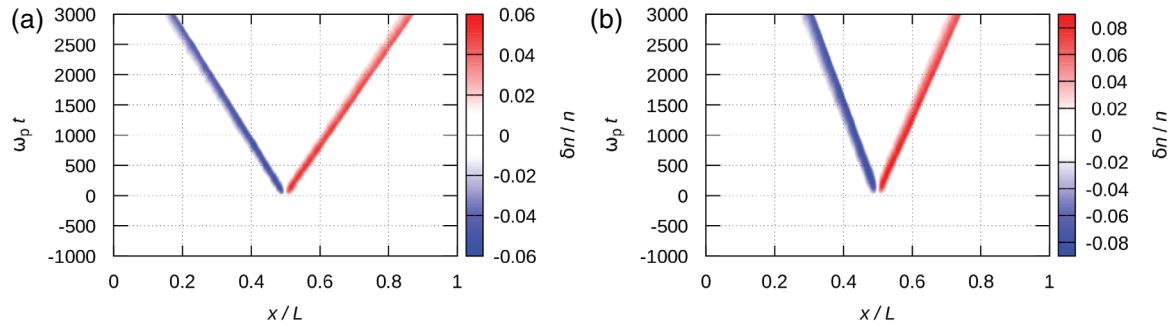


**FIGURE 4** Density of the system as a function of space and time for  $\Gamma = 100$  and (a)  $\kappa = 2$  and (b)  $\kappa = 3$ .  $\tilde{E}_0 = 0.554$ . The corresponding plot for  $\kappa = 1$  was shown in Figure 2b

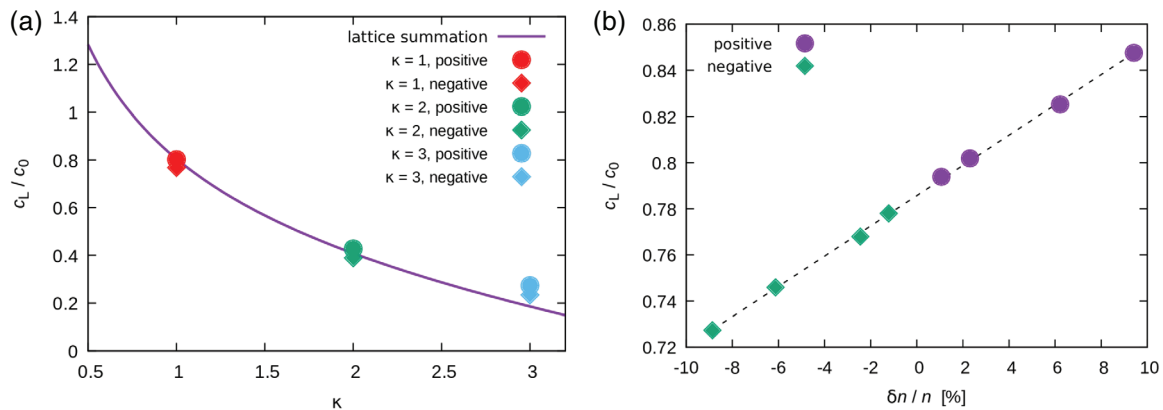


**FIGURE 5** Propagation velocity of the solitons: (a) dependence on the screening parameter  $\kappa$  at a fixed pulse amplitude  $\tilde{E}_0 = 0.554$  (symbols, data taken from Figure 4). The line shows the 2D Yukawa lattice sound speed as reference (approximate formula taken from ref. 67). The normalization factor is  $c_0 = \omega_p a$ . (b) Dependence on density modulation amplitude including both compressional (positive) and rarefactive (negative) waves (symbols, data taken from Figure 3) at  $\kappa = 1$ . The dashed line is a linear fit to the data points, shown to guide the eye

of the density perturbation  $\delta n/n$  (that in turn, depends on  $\tilde{E}_0$ ). The data indicate a linear dependence of the velocity on  $\delta n/n$ . This result is in good qualitative agreement with earlier experiments performed in a two-dimensional dusty plasma crystal,<sup>[39]</sup> where solitons were launched by laser pulses with different peak intensities.

Next, we investigate the scenario when the perturbing electric field is applied simultaneously at two locations in the simulation box (at  $x/L = 0.25$  and  $0.75$ ). Figure 6a shows the case when the electric field has the same polarity at the two different locations, while Figure 6b corresponds to the case when the electric field has opposite polarity at the two selected locations. In both cases, two pairs of solitons are generated. The plots of the density distributions confirm that the solitons cross each other without influencing each other's propagation.

### 3.2 | The effect of the magnetic field

Finally, we address the effect of an external magnetic field on the propagation of the solitons. In the first case, an external magnetic field with a strength of  $\beta = 0.1$  is turned on in the simulation at the time  $\omega_p t = 1333.3$ . Figure 7 shows that both the positive and negative peaks become trapped, they neither propagate nor dissolve by diffusion in the system over the time scale of the simulation. In the trapped state, the particles undergo a cyclotron-type motion characterized by the strength of the magnetic field ( $\beta$ ).

In Figure 8 we cover lower values of the magnetic field,  $\beta = 0.02$  and  $0.01$ . For these conditions we also observe the trapping of the density perturbations upon the application of the magnetic field, however at the same time, wave-like structures are also generated. Detailed understanding of these requires further studies.

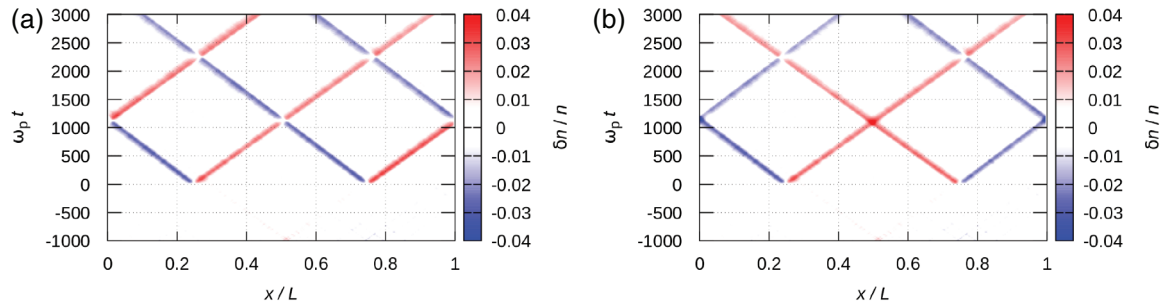


**FIGURE 6** Density of the system as a function of space and time for the cases of two pairs of solitons, generated at  $x/L = 0.25$  and at  $x/L = 0.75$ .  $|\tilde{E}_0| = 0.554$ ,  $\Gamma = 100$ ,  $\kappa = 1$ . In (a) the solitons are created at the two selected spatial positions by electric field pulse having the same polarity, while in (b) the polarity of the electric field pulses is opposite at the two locations

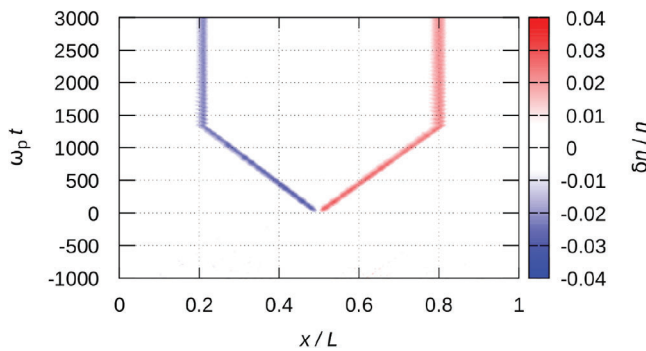


**FIGURE 7** Effect of magnetic field on the propagation of the solitons: a magnetic field with  $\beta = 0.1$  is turned on at  $\omega_p t = 1333.3$ .  $\Gamma = 100$ ,  $\kappa = 1$ ,  $\tilde{E}_0 = 0.554$ ,  $x_0/L = 0.5$ . Upon the application of the magnetic field the propagation of the pulses is blocked as the cyclotron motion converts propagation into localized oscillations

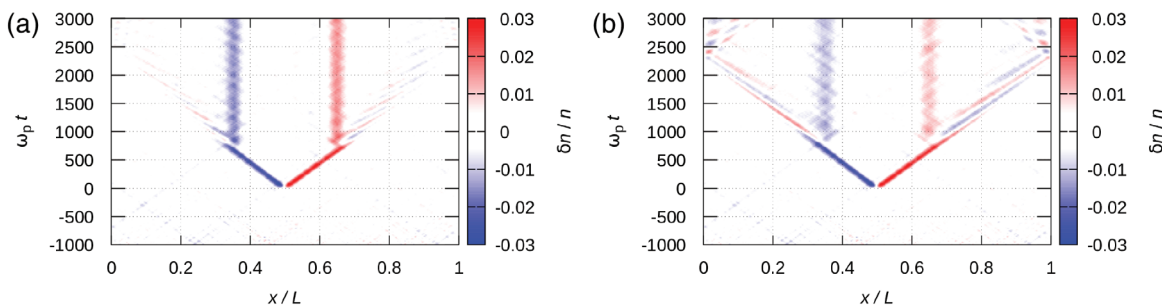


**FIGURE 8** Effect of magnetic field on the propagation of the solitons at (a)  $\beta = 0.02$  and (b)  $\beta = 0.01$ . The magnetic field is turned on at  $\omega_p t = 666.6$ .  $\Gamma = 100$ ,  $\kappa = 1$ ,  $\tilde{E}_0 = 0.554$ ,  $x_0/L = 0.5$

It is interesting to note that if the magnetic field is switched off after a certain time, the temporarily blocked solitons can be “released”. What happens at this moment is defined by the phase of the cyclotron motion. To illustrate this effect Figure 9 displays and Table 1 lists a sequence of cases with small differences in the magnetic field strength ( $\beta$ ).

Depending on the phase of the cyclotron oscillation of the trapped particles the solitons can (a) continue propagating into their original directions, termed as “transmission” in Table 1, (b) propagate into the opposite directions, termed as “reflection” in Table 1, as well as (c) split into a pair of solitons having the same polarity, termed as “splitting” in Table 1.

For the cases studied the on phase of the magnetic field pulse has a fixed duration of  $\omega_p T = 333.3$ . During this time the particles undergo a number of cyclotron oscillations  $N_c = \Omega_c T / 2\pi = 333.3(\Omega_c / \omega_p) / 2\pi = 333.3\beta / 2\pi$ . Along with the values of  $\beta$ , Table 1. also gives the values of  $N_c$  as defined above and its fractional part converted to a phase angle  $0^\circ \leq \phi \leq 360^\circ$ . Our data show that whenever  $\phi$  is close to  $0^\circ$  or  $360^\circ$ , the solitons are transmitted after the temporary trapping by the magnetic field pulse. Reflection occurs whenever  $\phi$  is in the vicinity of  $180^\circ$ , as expected because of the delay of phase of the localized cyclotron oscillations. At intermediate values of  $\phi$ , close to  $90^\circ$  and  $270^\circ$  splitting occurs with nearly equal or

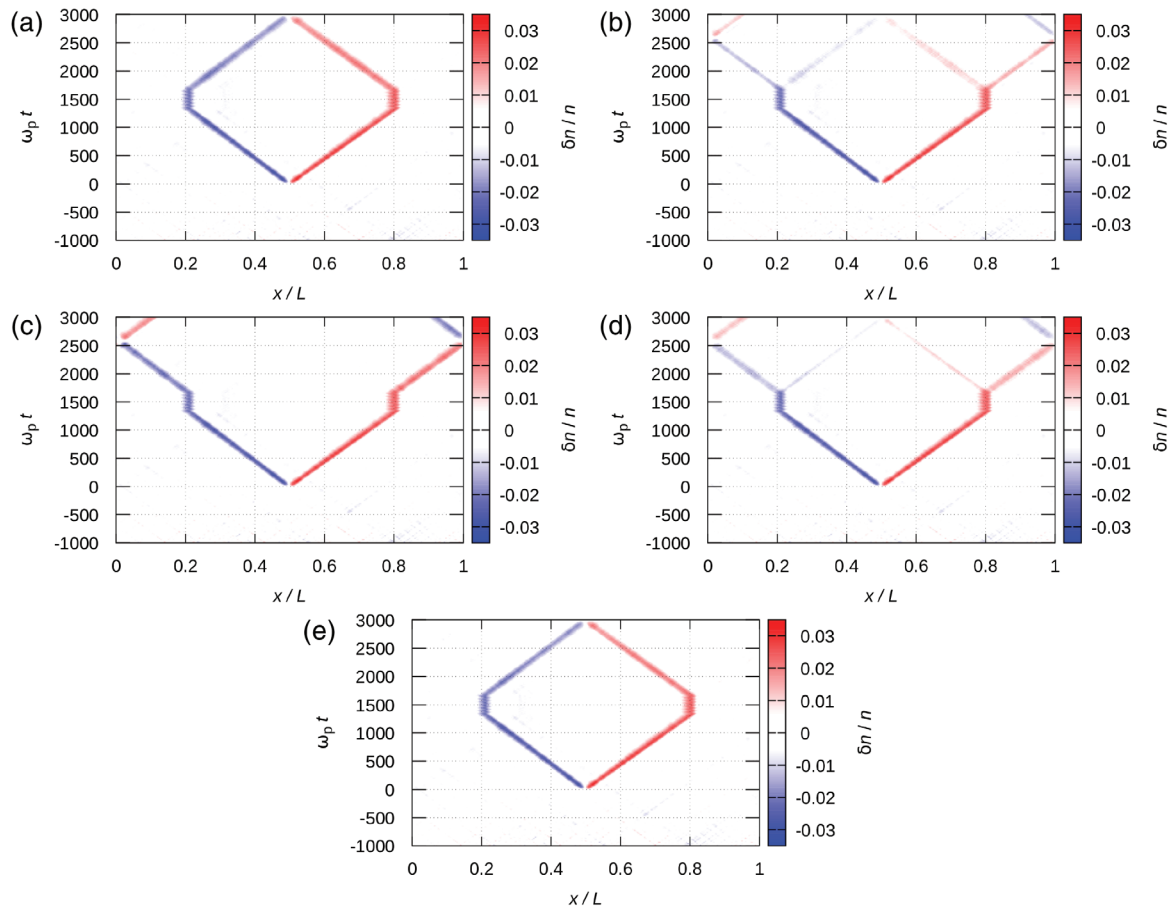


**FIGURE 9** Effect of a magnetic field pulse on soliton propagation: (a)  $\beta = 0.104$ , (b)  $\beta = 0.108$ , (c)  $\beta = 0.112$ , (d)  $\beta = 0.116$ , and (e)  $\beta = 0.120$ .  $\Gamma = 100$ ,  $\kappa = 1$ ,  $\tilde{E}_0 = 0.554$ . The magnetic field pulse has a duration of  $\omega_p T = 333.\dot{3}$ , subsequently the solitons are released and can propagate in their original, opposite, or both direction(s) depending on the magnetic field strength

**TABLE 1** Parameters of cases shown in Figure 9

$\beta$	$N_c$	$\phi$ ( $^\circ$ )	Effect	Figure
0.102	5.411	148.1	Reflection	
0.104	5.517	186.3	Reflection	8a
0.106	5.623	224.4	Splitting	
0.108	5.730	262.6	Splitting	8b
0.110	5.836	300.8	Transmission	
0.112	5.942	339.0	Transmission	8c
0.114	6.048	17.2	Transmission	
0.116	6.154	55.4	Splitting	8d
0.118	6.260	93.6	Splitting	
0.120	6.366	131.8	Reflection	8e
0.122	6.472	170.0	Reflection	
0.124	6.578	208.2	Reflection	

Note:  $\beta$  is the normalized magnetic field strength,  $N_c = \Omega_c T / 2\pi$  is the number of cyclotron oscillation cycles during the on phase of the magnetic field,  $\phi$  is the phase angle of the fractional part of  $N_c$ .

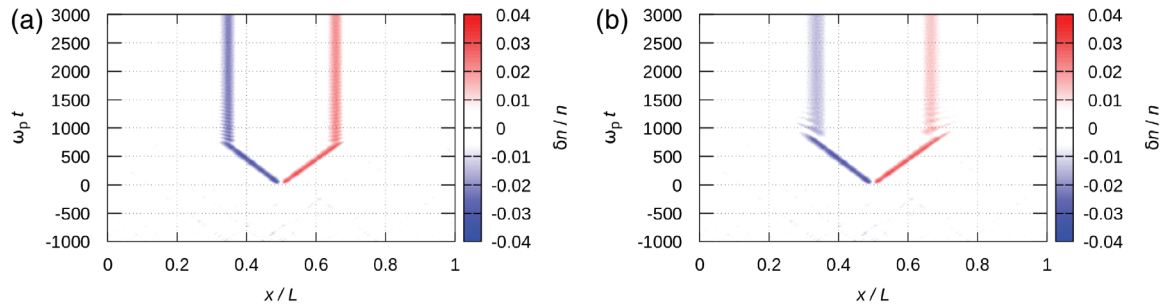


**FIGURE 10** Effect of magnetic field on the propagation of the solitons. The magnetic field is turned on at  $\omega_p t = 666.6$  and reaches the value of  $\beta = 0.1$  during ramp times of (a)  $\omega_p t = 166.6$  and (b)  $\omega_p t = 1,000$ .  $\Gamma = 100$ ,  $\kappa = 1$ ,  $\tilde{E}_0 = 0.554$ ,  $x_0/L = 0.5$

different amplitudes depending on the exact value of  $\phi$ . It is expected that the localization time (duration of the magnetic field pulse) has a similar effect as the effect of the magnetic field strength, as  $N_c$ , and consequently  $\phi$  are proportional to  $T$ .

Finally, we illustrate the more realistic scenario when the magnetic field is not turned on instantly, but it reaches its stationary value with a finite rate. Simulation results based on this approach are shown in Figure 10. Panel a corresponds to a ramp time of  $\omega_p t = 166.6$ , while panel b corresponds to  $\omega_p t = 1,000$ . The shorter ramp time results basically in the same scenario as observed in the case of “instant” application of the magnetic field. This observation also implies that most of our findings can be expected to be valid under the conditions when the magnetic field reaches its stationary value during a (not very long) ramp phase. In the case of a slower ramp, shown in Figure 10b we observe the emergence of additional “wings” in the density profiles that gradually smear with the increase of the magnetic field. Understanding the fine structures of these details is beyond the scope of the paper.

## 4 | SUMMARY

This work reported our investigations on the propagation of solitons, created by electric field pulses, in a two-dimensional strongly coupled many body system characterized by the Yukawa potential. The electric field pulses created a pair of solitons, with positive / negative density peaks (referenced to the density of the unperturbed system) that were found to propagate into opposite directions. The propagation speed of both features in the limit of small density perturbations was found to be equal to the longitudinal sound speed in the Yukawa liquid. With increasing perturbation, the propagation speed of the positive peak was found to increase, while the propagation speed of the negative peak was found to decrease.

An external magnetic field was found to “freeze” the positions of the density peaks (solitons) due to the largely reduced self-diffusion in the system at  $\beta > 0$ . Upon the termination of this magnetic field, however, the solitons were found to be released from these “traps” and to continue propagating into directions that depends on the strength of the magnetic field and the trapping time. These observations and the dynamics of the system at low magnetic fields as well as in the case of a ramp-like application of the magnetic field call for further studies at the microscopic level of individual particles. The exploration of multiple solitons trapped simultaneously by magnetic field pulses is also identified as an interesting topic for future work.

## ACKNOWLEDGMENTS

This work has been supported by the Hungarian Office for Research, Development, and Innovation (NKFIH 119357 and 115805) and by the grant AP05132665 of the Ministry of Education and Science of the Republic of Kazakhstan.

## REFERENCES

- [1] J. Robinson and J. Russel, Report of the Committee on Waves, Report of the 7th Meeting of British Association for the Advancement of Science, (Liverpool, London, John Murray, **1838**).
- [2] J. S. Russell, Report on Waves: Made to the Meetings of the British Association in 1842–43 (Creative Media Partners, LLC, 1845 and 2018) **2019**.
- [3] D. D. J. Korteweg, D. G. de Vries, *London Edinburgh Dublin Philos. Mag. J. Sci*002E **1895**, 39(240), 422.
- [4] A. Hasegawa, F. Tappert, *Appl. Phys. Lett.* **1973**, 23, 142.

- [5] A. M. Kosevich, V. V. Gann, A. I. Zhukov, V. P. Voronov, *J. Exp. Theor. Phys.* **1998**, 87(2), 401.
- [6] Y. Iwata, P. Stevenson, *New J. Phys.* **2019**, 21(4), 043010.
- [7] D. J. Frantzeskakis, *J. Phys. A Math. Theor.* **2010**, 43(21), 213001.
- [8] M. Q. Tran, *Physica Scripta* **1979**, 20(3–4), 317.
- [9] C. P. Olivier, F. Verheest, W. A. Hereman, *Phys. Plasmas* **2018**, 25(3), 032309.
- [10] F. Verheest, W. A. Hereman, *J. Plasma Phys.* **2019**, 85(1), 905850106.
- [11] E. EL-Shamy, E. El-Shewy, N. Abdo, M. O. Abdellahi, O. Al-Hagan, *Contrib. Plasma Phys.* **2019**, 59(3), 304.
- [12] H. Ur-Rehman, S. Mahmood, *Contrib. Plasma Phys.* **2019**, 59(2), 236.
- [13] M. S. Alam, M. R. Talukder, *Contrib. Plasma Phys.* **2019**, 59(0), e201800163.
- [14] A. M. Wazwaz, *Chaos Solitons Fractals* **2015**, 76, 93.
- [15] N. S. Saini, B. Kaur, T. S. Gill, *Phys. Plasmas* **2016**, 23(12), 123705.
- [16] A. Atteya, S. Sultana, R. Schlickeiser, *Chin. J. Physics* **2018**, 56(5), 1931.
- [17] M. E. Yahia, S. K. El-Labany, R. Sabry, W. M. Moslem, E. A. Elghmaz, *IEEE Trans. Plasma Sci.* **2019**, 47, 762.
- [18] Y. Y. Wang, J. T. Li, C. Q. Dai, X. F. Chen, J. F. Zhang, *Phys. Lett. A* **2013**, 377(34), 2097.
- [19] A. Mukherjee, M. S. Janaki, A. Kundu, *Phys. Plasmas* **2015**, 22(12), 122114.
- [20] H. Ishihara, K. Matsuno, M. Takahashi, S. Teramae, *Phys. Rev. D* **2018**, 98(Dec), 123010.
- [21] D. Samsonov, A. V. Ivlev, R. A. Quinn, G. Morfill, S. Zhdanov, *Phys. Rev. Lett.* **2002**, 88(Feb), 095004.
- [22] V. Nosenko, K. Avinash, J. Goree, B. Liu, *Phys. Rev. Lett.* **2004**, 92, 085001.
- [23] V. Nosenko, J. Goree, F. Skiff, *Phys. Rev. E* **2006**, 73, 016401.
- [24] T. E. Sheridan, V. Nosenko, J. Goree, *Phys. Plasmas* **2008**, 15(7), 073703.
- [25] P. Bandyopadhyay, G. Prasad, A. Sen, P. K. Kaw, *Phys. Rev. Lett.* **2008**, 101(Aug), 065006.
- [26] R. Heidemann, S. Zhdanov, R. Sütterlin, H. M. Thomas, G. E. Morfill, *Phys. Rev. Lett.* **2009**, 102(Mar), 135002.
- [27] S. Zhdanov, R. Heidemann, M. H. Thoma, R. Sütterlin, H. M. Thomas, H. Höfner, K. Tarantik, G. E. Morfill, A. D. Usachev, O. F. Petrov, V. E. Fortov, *Europhys. Lett.* **2010**, 89(2), 25001.
- [28] A. Boruah, S. K. Sharma, H. Bailung, Y. Nakamura, *Phys. Plasmas* **2015**, 22(9), 093706.
- [29] G. Arora, P. Bandyopadhyay, M. G. Hariprasad, A. Sen, *Phys. Plasmas* **2019**, 26(9), 093701.
- [30] A. Usachev, A. Zobnin, O. Petrov, V. Fortov, M. H. Thoma, H. Höfner, M. Fink, A. Ivlev, G. Morfill, *New J. Phys.* **2014**, 16(5), 053028.
- [31] T. E. Sheridan, J. C. Gallagher, *J. Plasma Phys.* **2017**, 83(3), 905830305.
- [32] A. Berbri, M. Tribeche, *Phys. Plasmas* **2009**, 16(5), 053703.
- [33] M. Nouri Kadijani, H. Zaremoghaddam, *J. Fusion Energy* **2012**, 31(5), 455.
- [34] P. Chatterjee, R. Ali, A. Saha, *Zeitschrift für Naturforschung A* **2018**, 73(2), 151.
- [35] M. Rahman, N. Chowdhury, A. Mannan, M. Rahman, A. Mamun, *Chin. J. Phys.* **2018**, 56(5), 2061.
- [36] N. Paul, K. Mondal, P. Chatterjee, *Z. Naturforsch. A* **2019**, 74(0), 861.
- [37] D. N. Gao, Z. R. Zhang, J. P. Wu, D. Luo, W. S. Duan, Z. Z. Li, *Braz. J. Phys.* **2019**, 49(5), 693.
- [38] K. N. Dzhumagulova, T. S. Ramazanov, R. U. Masheeva, *Contrib. Plasma Phys.* **2012**, 52(3), 182.
- [39] K. Avinash, P. Zhu, V. Nosenko, J. Goree, *Phys. Rev. E* **2003**, 68, 046402.
- [40] S. Kumar, S. K. Tiwari, A. Das, *Phys. Plasmas* **2017**, 24(3), 033711.
- [41] S. K. Tiwari, A. Sen, *Phys. Plasmas* **2016**, 23(10), 100705.
- [42] S. K. Tiwari, A. Das, A. Sen, P. Kaw, *Phys. Plasmas* **2015**, 22(3), 033706.
- [43] J. H. Chu, I. Lin, *Phys. Rev. Lett.* **1994**, 72, 4009.
- [44] H. Thomas, G. E. Morfill, V. Demmel, J. Goree, B. Feuerbacher, D. Möhlmann, *Phys. Rev. Lett.* **1994**, 73, 652.
- [45] A. Melzer, T. Trottenberg, A. Piel, *Phys. Lett. A* **1994**, 191(3), 301.
- [46] S. D. Baalrud, J. Daligault, *Phys. Rev. E* **2017**, 96, 043202.
- [47] Y. Feng, W. Lin, M. S. Murillo, *Phys. Rev. E* **2017**, 96, 053208.
- [48] P. Hartmann, J. C. Reyes, E. G. Kostadinova, L. S. Matthews, T. W. Hyde, R. U. Masheeva, K. N. Dzhumagulova, T. S. Ramazanov, T. Ott, H. Kählert, M. Bonitz, I. Korolov, Z. Donkó, *Phys. Rev. E* **2019**, 99, 013203.
- [49] B. Scheiner, S. D. Baalrud, *Phys. Rev. E* **2019**, 100(Oct), 043206.
- [50] J. K. Meyer, I. Laut, S. K. Zhdanov, V. Nosenko, H. M. Thomas, *Phys. Rev. Lett.* **2017**, 119, 255001.
- [51] S. Kumar, A. Das, *Phys. Rev. E* **2018**, 97, 063202.
- [52] W. Li, D. Huang, K. Wang, C. Reichhardt, C. J. O. Reichhardt, M. S. Murillo, Y. Feng, *Phys. Rev. E* **2018**, 98, 063203.
- [53] C. S. Wong, J. Goree, Z. Haralson, *Phys. Rev. E* **2018**, 98(Dec), 063201.
- [54] N. P. Kryuchkov, E. V. Yakovlev, E. A. Gorbunov, L. Couëdel, A. M. Lipaev, S. O. Yurchenko, *Phys. Rev. Lett.* **2018**, 121, 075003.
- [55] H. W. Hu, W. Wang, and L. I, *Phys. Rev. Lett.* **123**, 065002 (2019).
- [56] P. Hartmann, A. Douglass, J. C. Reyes, L. S. Matthews, T. W. Hyde, A. Kovács, Z. Donkó, *Phys. Rev. Lett.* **2010**, 105(Sep), 115004.
- [57] Y. S. Su, C. W. Io, I. Lin, *Phys. Rev. E* **2012**, 86, 016405.
- [58] O. F. Petrov, M. M. Vasiliev, Y. Tun, K. B. Statsenko, O. S. Vaulina, E. V. Vasilieva, V. E. Fortov, *J. Exp. Theor. Phys.* **2015**, 120(2), 327.
- [59] S. Jaiswal, E. Thomas, *Plasma Res. Express* **2019**, 1(2), 025014.
- [60] K. Wang, D. Huang, Y. Feng, *Phys. Rev. E* **2019**, 99, 063206.
- [61] M. Himpel, A. Melzer, *Phys. Rev. E* **2019**, 99, 063203.
- [62] Y. Choi, G. Dharuman, M. S. Murillo, *Phys. Rev. E* **2019**, 100, 013206.

- [63] I. I. Lisina, O. S. Vaulina, E. A. Lisin, *Phys. Rev. E* **2019**, *99*, 013207.
- [64] G. I. Sukhinin, A. V. Fedoseev, M. V. Salnikov, A. Rostom, M. M. Vasiliev, O. F. Petrov, *Phys. Rev. E* **2017**, *95*, 063207.
- [65] P. Hartmann, J. C. Reyes, I. Korolov, L. S. Matthews, T. W. Hyde, *Phys. Plasmas* **2017**, *24*(6), 060701.
- [66] Q. Spreiter, M. Walter, *J. Comput. Phys.* **1999**, *152*(1), 102.
- [67] I. L. Semenov, S. A. Khrapak, H. M. Thomas, *Phys. Plasmas* **2015**, *22*(11), 114504.

**How to cite this article:** Donkó Z, Hartmann P, Masheyeva RU, Dzhumagulova KN. Molecular dynamics investigation of soliton propagation in a two-dimensional Yukawa liquid. *Contributions to Plasma Physics*. 2020;e201900197. <https://doi.org/10.1002/ctpp.201900197>